applied optics

Krypton tagging velocimetry of an underexpanded jet

N. J. Parziale,[1,*] M. S. Smith,[2] and E. C. Marineau[3]

[1]Mechanical Engineering, Stevens Institute of Technology, Castle Point on Hudson, Hoboken, New Jersey 07030, USA
[2]Aerospace Testing Alliance, Silver Spring, Maryland 20903, USA
[3]AEDC White Oak, Silver Spring, Maryland 20903, USA
*Corresponding author: nick.parziale@gmail.com

Received 25 February 2015; revised 30 April 2015; accepted 30 April 2015; posted 1 May 2015 (Doc. ID 232446); published 28 May 2015

In this work, we present the excitation/emission strategy, experimental setup, and results of an implementation of krypton tagging velocimetry (KTV). KTV is performed as follows: (i) seed a base flow with krypton; (ii) photosynthesize metastable krypton atoms with a frequency-doubled dye laser to form the tagged tracer; (iii) record the translation of the tagged metastable krypton by imaging the laser-induced fluorescence (LIF) that is produced with an additional dye laser. The principle strength of KTV, relative to other tagging velocimetry techniques, is the use of a chemically inert tracer. KTV results are presented for an underexpanded jet of three mixtures of varying Kr/N_2 concentration. It is demonstrated that KTV can be used in gas mixtures of relatively low krypton mole fraction (0.5% Kr/99.5% N_2), and the KTV data from that experiment are found to be in good agreement with an empirical fit found in the literature. We find that KTV is useful to perform instantaneous velocity measurements with metastable krypton as a chemically inert, dilute, long-lifetime tracer in gas-phase flows.

OCIS codes: (120.7250) Velocimetry; (280.7250) Velocimetry; (300.2530) Fluorescence, laser-induced; (280.4788) Optical sensing and sensors; (280.2490) Flow diagnostics; (300.6280) Spectroscopy, fluorescence and luminescence.

http://dx.doi.org/10.1364/AO.54.005094

1. INTRODUCTION

Velocimetry techniques for use in high-speed wind-tunnel facilities are of interest to study flow fields for the purposes of thermal/fluids science and test and evaluation. These investigations are intended to further the understanding of the fundamental flow physics that influence macro-scale behavior of test articles. Researchers have developed various forms of velocimetry techniques; for examples, see the handbook edited by Tropea *et al.* [1]. In that handbook, there is a chapter [2] that describes the basics of tagging velocimetry.

The methodology of tagging velocimetry is similar to observing the translation of a dye that has been introduced to a fluid; the dye is used as a tracer in the fluid and observed at prescribed times. In tagging velocimetry of gas-phase flows, the tracer is a native, seeded, or synthesized gas. Typically, fluorescence of the tracer is induced to provide spatial information at prescribed times so that velocity may be obtained.

In this work, we present metastable krypton as a candidate tracer for tagging velocimetry. First, we motivate the use of Kr by reviewing the characteristics of tracers that have been reported in the literature. Then, we present the krypton excitation/emission strategy, experimental setup, and results of an implementation of krypton tagging velocimetry (KTV) as applied to an underexpanded jet of three mixtures. Finally, the KTV results are reduced and compared to an appropriate correlation of historical data.

2. REVIEW OF EXISTING GAS-PHASE TRACERS

Different constituents can be used as the tagging medium in high-speed gas flows. Important characteristics of tracers included: lifetime, reactivity, intensity of fluorescence, and ease of seeding/synthesis and excitation.

Oxygen may be used as an unseeded tracer in air and O_2 flows or possibly partially dissociated CO_2 flows. The Raman excitation plus laser-induced electronic fluorescence (RELIEF) technique [3–7] utilizes vibrationally excited O_2 as a tracer, and has a lifetime that is a function of the vibrational relaxation time. Researchers report the use of a dye laser and an ArF laser to implement RELIEF. Other researchers have used oxygen as a tracer by photochemically creating ozone, photodissociating the ozone to form O_2, and imaging laser-induced fluorescence (LIF) from the O_2 [8–10]. The ozone tracer is reported to have a lifetime on the order of seconds.

Nitrogen can be used as an unseeded tracer in air and N_2 flows. In Michael *et al.* [11], the tracer was created by nonlinear excitation and dissociation of nitrogen with a femtosecond laser.

Spatial information is recorded by imaging the emission of the recombining nitrogen atoms. In that work, researchers report an effective tracer lifetime on the order of 10 μs.

Nitric oxide (NO) is an attractive candidate as a tracer for reasons including its long lifetime (order 1–10 ms in the absence of polyatomic molecules) and ease of *in situ* production/seeding. The air photolysis and recombination technique (APART) technique [12–14] entails the photosynthesis of NO from N_2 and O_2 by an ArF excimer laser. Then, a tunable pulsed laser is used to induce fluorescence from the tagged NO. Researchers have utilized the photodissociation of seeded $(CH_3)_3CONO$ [15], NO_2 [16–23], or N_2O [24] to produce NO, and subsequently image LIF for time-of-flight velocimetry. Additionally, researchers have also utilized direct NO seeding for velocimetry [25–29]. Furthermore, researchers have performed experiments in shocktunnels with prescribed shocktube mixtures (≈99% N_2 ≈1% O_2) to create an appropriate concentration of NO (≈1%) in the free-stream for velocimetry [30–32]. It should be noted that the vibrationally excited nitric oxide monitoring (VENOM) technique [17–20,29] is also capable of simultaneous temperature measurements.

Other tracers include iodine [33,34], acetone [35–37], and the hydroxyl group [38–40], among others [41–44]. These schemes generally require seeding or *in situ* production of the tracer.

3. MOTIVATION FOR EXPLORATION OF KRYPTON AS A TRACER

We focus our efforts on tagging velocimetry with photosynthesized metastable krypton as a chemically inert tracer, as proposed by Mills *et al.* [45] and Balla and Everhart [46]. Mills *et al.* proposed that krypton tagging velocimetry could be performed as follows:

1. *Write* tracer line by two-photon excitation, $4p^6(^1S_0) \rightarrow 6p[3/2]_2$ (193 nm) with an ArF laser.
2. *Decay* to metastable state, $6p[3/2]_2 \rightarrow 5s[3/2]_2^o$ (427.4 nm).
3. *Excite* $5p[5/2]_3$ level by $5s[3/2]_2^o \rightarrow 5p[5/2]_3$ (811.3 nm) with a diode laser.
4. *Read* spontaneous emission of $5p[5/2]_3 \rightarrow 5s[3/2]_2^o$ (811.3 nm) transitions with a camera positioned normal to the flow.

This approach would permit time-of-flight velocimetry measurements. However, we are not restricted to the creation of metastable Kr atoms with an ArF laser through the $4p^6(^1S_0) \rightarrow 6p[3/2]_2 \rightarrow 5s[3/2]_2^o$ transition strategy. A disadvantage of this method is the need for an ArF laser, which requires specialized maintenance. Alternatively, Narayanaswamy *et al.* [47] used two-photon excitation of the $5p[3/2]_2$ level by sum-frequency mixing the output of a dye laser and a frequency tripled Nd:YAG laser. Following excitation there is decay via the $5p[3/2]_2 \rightarrow 5s[3/2]_1^o$ and $5p[3/2]_2 \rightarrow 5s[3/2]_2^o$ transitions. Narayanaswamy *et al.* used this excitation/emission strategy for Kr planar laser-induced fluorescence (PLIF) work for flow visualization and scalar imaging of an underexpanded jet of 100% krypton. This is the write-excitation strategy we will use in this work. In addition, please note that Racah $nl[K]_J$ notation is used throughout this paper.

The fundamental strength of KTV is that the tracer (metastable krypton) is chemically inert. The nonreactive nature of Kr is in contrast to other tracers that represent the current state of the art. This may enable the technique to be employed in a wide variety of environments because the seeded krypton atoms are nominally independent of chemical processes that may occur in the bulk flow. Because of this flexibility, KTV demonstrates the potential to broaden the usefulness of tagging velocimetry with new applications to reacting gas-phase flows, including combustion and nonequilibrium gasdynamics. Moreover, Hsu *et al.* [48] review some benefits of using Kr as a medium. The atomic structure is well known [49], and relative to other noble gases, two-photon excitation is accessible with commercially available laser and optical components.

KTV may prove particularly useful where the chemical composition of the flow field evolves, or is difficult to prescribe or predict. For example, in high-enthalpy aerodynamics work, it is typical for researchers to investigate thermochemical/fluid-mechanic interaction by studying and comparing flows with gases that are more thermochemically active (e.g., CO_2 or air) and less thermochemically active (e.g., N_2). It may be possible for krypton to be used as a dilute tracer in CO_2, air, or N_2; so, the researcher would not have to change velocimetry diagnostics to investigate different gasses about the same body.

Miles and Lempert [6] write that one "limitation [of tagging velocimetry] has to do with the lifetime of the tagged molecules. Of particular importance are collisions with polyatomic molecules such as water, carbon dioxide, and in combustion applications, fuels such as methane and other hydrocarbons." However, the prospect of using KTV in flows with polyatomic molecules is promising. Buxton *et al.* [50] and Hsu *et al.* [48] have utilized Kr for PLIF work in combustion environments with Kr seeding mole fractions of ≈1–4%. These researchers also note that the low seeding mole fractions "avoided disturbance of the flame." Researchers report the metastable state has a lifetime on the order of seconds [51,52]. However, in those fundamental science experiments, the temperature, pressure, and surrounding environment are markedly different than in flows of interest in combustion and aerothermodynamics applications. Researchers have studied the quenching rates of the $5s[3/2]_2^o$ state with a number of collisional partners [53–56]. Using the quenching rate constant from Velazco *et al.* [54] for metastable krypton in N_2, a lifetime on the order of 10 μs is estimated for conditions typical of the underexpanded jet used as the flowfield to demostrate KTV in this work; therefore, the lifetime of the $5s[3/2]_2^o$ state should be sufficient.

Krypton gas-bottle cost is appropriate for laboratory-scale KTV efforts. Estimates indicate that the seeding cost per run of 1% Kr mole fraction ranges from ≈10 USD in impulse facilities (e.g., Ludwieg tubes, shocktunnels, and moderate reservoir pressure blow-down facilities) to ≈100 USD in high reservoir pressure long-duration blow-down hypersonic tunnels (e.g., Tunnel 9 at AEDC White Oak [57]).

Assuming that the krypton may be seeded into the flow in dilute concentrations, the thermo-physical properties of the flow are nominally unchanged. Estimates of the effect of dilute krypton concentrations on the transport properties can be

performed using Cantera [58] via the semi-empirical Chapman–Enskog method [59] with the appropriate thermodynamic data [60–62]. For example, if N_2 is seeded with 1% Kr mole fraction at 300 K and 1 atm, the Reynolds, Prandtl, Lewis, and Peclet numbers and the ratio of specific heats are changed by ≈0.1–0.3%. Additionally, the Schmidt number of the tagged krypton is approximately the same (≈1) as other tagging schemes that utilize nitrogen, oxygen, or nitrogen oxide; therefore, the concern of the molecular diffusion of the tracer in KTV is similar to the other gas-phase tagging candidates.

4. EXCITATION/EMISSION STRATEGY

To use metastable krypton as a tracer in a gas flow field, pulsed tunable lasers can be used to excite and/or induce fluorescence of Kr atoms that have been seeded into the flow for the purposes of position tracking. An energy level diagram for the KTV scheme is presented as Fig. 1. The excitation/emission strategy is as follows:

1. *Write* tracer line by two-photon excitation of $4p^6(^1S_0) \rightarrow 5p[3/2]_2$ (214.7 nm).
2. *Decay* to metastable states $5p[3/2]_2 \rightarrow 5s[3/2]_1^o$ (819.0 nm) and $5p[3/2]_2 \rightarrow 5s[3/2]_2^o$ (760.2 nm).
3. *Excite* $5p[3/2]_2$ level by $5s[3/2]_2^o \rightarrow 5p[3/2]_2$ transition with laser sheet (760.2 nm).
4. *Read* spontaneous emission of $5p[3/2]_2 \rightarrow 5s[3/2]_1^o$ (819.0 nm) and $5p[3/2]_2 \rightarrow 5s[3/2]_2^o$ (760.2 nm) transitions with a camera positioned normal to the flow.

Miller [63] reports two-photon excitation of the $5p[3/2]_2$ level in Kr at 214.7 nm, which corresponds to the $4p^6(^1S_0) \rightarrow 5p[3/2]_2$ transition. The same work reports that the branching fraction for the $5p[3/2]_2 \rightarrow 5s[3/2]_1^o$ and $5p[3/2]_2 \rightarrow 5s[3/2]_2^o$ decay transitions are 27% and 73%, respectively. We choose the $5s[3/2]_2^o \rightarrow 5p[3/2]_2$ (760.2 nm) transition for read-excitation because of the favorable branching fraction during decay to obtain a strong signal-to-noise ratio (SNR). The $5p[3/2]_2 \rightarrow 5s[3/2]_1^o$ and $5p[3/2]_2 \rightarrow 5s[3/2]_2^o$ transitions occur on a time scale of approximately 20–35 ns [64–67].

5. EXPERIMENTAL SETUP

To demonstrate the KTV technique, an underexpanded jet is used as the flow field. The jet-orifice diameter is $D_j = 2$ mm. This jet was exhausted into a test cell, which was continuously evacuated to maintain an ambient pressure of approximately 7 torr. Well-mixed gas mixtures for the jet were created in a pressure vessel. A gas-pressure regulator was used to control the effective plenum pressure of the underexpanded jet, and a high-speed solenoid (ITT S31 series) was used to pulse the jet for 25 ms, beginning 20 ms prior to the write-laser pulse. The time scale associated with establishment of steady flow is estimated to be 10 ms, as formulated in Smith [68]. There is optical access to the test cell through three fused silica windows; two windows permit the read and write beams to enter and leave the test cell, and the third window is positioned at 90° to the other two windows to permit imaging. A block diagram of the experimental setup is presented as Fig. 2.

The write excitation was performed with a frequency doubled Continuum ND6000 Dye Laser, which was pumped with 400 mJ/pulse at 355 nm from a frequency tripled continuum PR8010 Nd:YAG laser. The dye was Coumarin 440 (Exciton). Frequency doubling of the dye-laser output (429.4 nm) was performed with an Inrad BBO-C (65°) crystal placed in a Inrad 820-360 gimbal mount. The 214.7 nm and 429.4 nm beams were separated with a Pellin–Broca prism. The 429.4 nm beam is sent to a beam dump and the 214.7 nm beam is focused to a narrow waist (≈40 μm in diameter) in the test section over the jet with a 600 mm fused silica lens (Fig. 3 left). This setup resulted in an approximately 1 mJ/pulse, with a wavelength of 214.7 nm, a linewidth of approximately 10 cm^{-1}, a pulsewidth of approximately 7 ns, and a repetition rate of 10 Hz. Assuming a Gaussian beam, the peak beam fluence is approximately 40 J/cm^2.

The read excitation was performed with a Continuum ND60 dye laser, which was pumped with approximately 250 mJ/pulse at 532 nm from a frequency doubled Continuum NY82S-10 Nd:YAG laser. The dye was LDS 765 (Exciton). This setup resulted in an approximately 10 mJ/pulse with a wavelength of 760.15 nm, a linewidth of approximately 10 cm^{-1}, a pulsewidth of approximately 8 ns, and a repetition rate of 10 Hz. The 760.15 nm beam is focused to a sheet (≈150 μm thickness) over the jet (Fig. 3 right). The read sheet overlaps the position of the write line and the position of the tagged Kr after it has been advected by the flow.

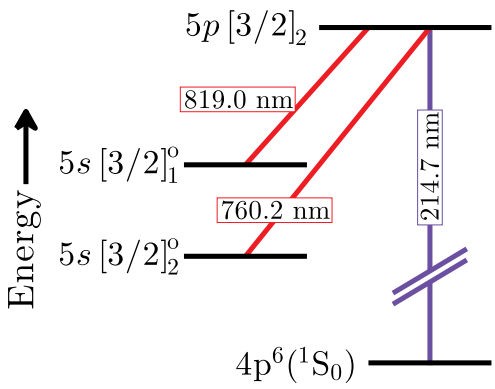

Fig. 1. Energy level diagram for KTV.

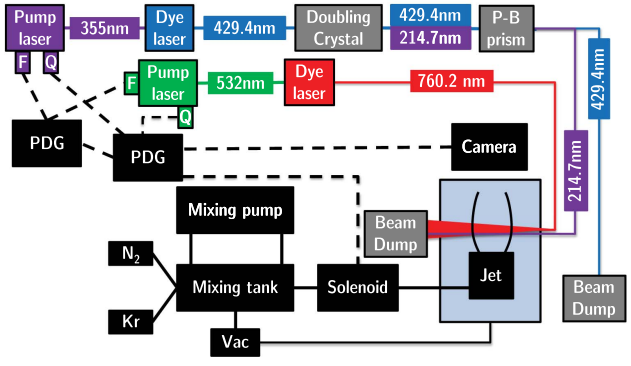

Fig. 2. Block diagram of experimental setup. Dashed lines indicate wiring. Solid lines indicate plumbing. Valves are not indicated. PDG, pulse delay generator; P-B prism, Pellin–Broca prism; F, flashlamp; Q, *Q*-switch; Vac, vacuum. Not to scale or indicative of plane.

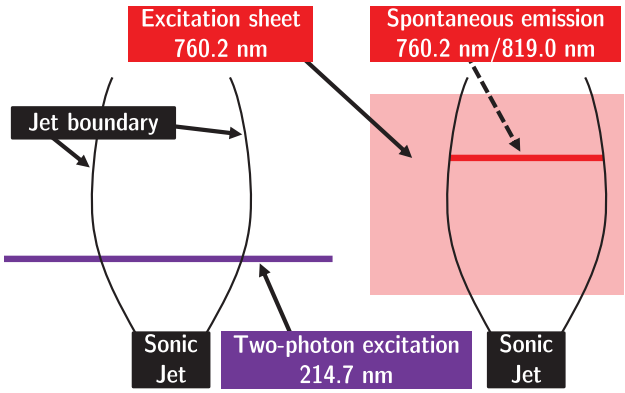

Fig. 3. Left: Schematic of the jet and the write line, which is purple and indicated by the solid arrow marking 214.7 nm. Right: Schematic of the jet and the read-excitation sheet, which is red and indicated by the solid arrow marking 760.2 nm. Additionally, on right is the spontaneous emission line from the tagged advected and excited Kr atoms, which is indicated by the dashed arrow marking 760.2 nm/819.0 nm emission. The object plane of the intensified camera is parallel to the page and coincident with the read sheet.

The timing is controlled by two pulse/delay generators. One pulse/delay generator (SRS DG535) is cycled internally at 10 Hz, and is used to trigger the flash lamps in the Nd:YAG lasers and a second pulse/delay generator. The second pulse/delay generator (BNC 505-4C) is run in single-shot mode and actively controls the two Q-switches in the Nd:YAG lasers, and triggers the solenoid and the gate for the intensified camera. The intensified camera is a 16-bit Princeton Instruments PIMAX-2 1024 × 1024 with a 18 mm Gen III Extended Blue intensifier; the gain is set to 255 for all experiments.

Each raw image recorded with the intensified camera is processed with MATLAB in three steps: (1) cropping the image to a region of interest around the flow field; (2) inverting the intensity scale by taking the compliment of each image; and (3) mapping the intensity values in each image to new values such that 1% of data is saturated at low and high intensities.

6. RESULTS

We present KTV results performed on an underexpanded jet for three cases of different Kr/N_2 mole fraction: Case 1: 100% Kr, Case 2: 5% Kr/95% N_2, and Case 3: 0.5% Kr/99.5% N_2. The underexpanded jet is pulsed, and after a fixed time delay the metastable krypton tracer is photosynthesized or written with the first laser at 214.7 nm. Then, the read sheet at 760.2 nm is pulsed at a further prescribed delay. This approach results in an observed distance of travel (by imaged LIF) for the metastable krypton tracer for a specified time.

The conditions at the write location of the underexpanded jet are calculated with an empirical fit found in Crist *et al.* [69] and presented in Table 1. Crist *et al.* [69] gives a relation for the Mach number M, as a function of distance from the jet orifice x, jet diameter D_j, and ratio of specific heats γ. The velocity is found by calculating the sound speed at each Mach number from the isentropic gas relations [70]. The molecular weight and the ratio of specific heats for the mixtures are computed with Cantera [58].

In Case 1, we present KTV in a 100% krypton underexpanded jet. The metastable krypton tracer is written approximately two diameters from the jet orifice. The effective plenum pressure is approximately 240 kPa. A series of four exposures is presented as Fig. 4. The KTV exposures show the compression waves at the jet boundary because of the long camera gate time (20 μs). For this series of experiments, the camera gate overlaps the write and read laser pulses. As the time delay between the write line and the read sheet is increased, there is an apparent translation of the tagged metastable Kr tracer. The decay in intensity of the spontaneous emission from the tagged Kr is also apparent. This indicates that the metastable state is decaying and/or the local number density is decreasing.

For Case 2, we present KTV of an underexpanded jet comprised of a 5% Kr/95% N_2 mole fraction mixture. The metastable krypton tracer is written approximately two diameters from the jet orifice. The effective plenum pressure is approximately 180 kPa. A series of four exposures is presented as Fig. 5. In this series, the camera gate (100 ns) is chosen to bracket only the spontaneous emission from the tagged Kr tracer (after the first image). In the first image, the camera gate overlaps the read and write pulses because they are pulsed at the same time. This is apparent when comparing the image sequences in Figs. 4 and 5. The laser induced fluorescence is not present at the bottom of each exposure in Fig. 5 because of the chosen camera gate.

For Case 3, we present KTV of an underexpanded jet comprised of a 0.5% Kr/99.5% N_2 mole fraction mixture. The metastable krypton tracer is written approximately two diameters from the jet orifice. The effective plenum pressure is approximately 180 kPa. A series of six exposures is presented

Table 1. Conditions of the Underexpanded Jet for each of the Three Cases with a Fictitious Fourth Case of Pure N_2[a]

Case	X_{Kr}	X_{N_2}	P_R	W	P_w	ρ_w	V_w	M_w	γ_w	Re_w^{unit}	Pr_w
	(–)	(–)	(kPa)	(g/mol)	(Pa)	(kg/m^3)	(m/s)	(–)	(–)	(1/m)	(–)
1, Fig. 4	1.000	0.000	240	83.8	491	0.200	507	5.72	1.67	56.7e6	0.667
2, Fig. 5	0.050	0.950	180	30.8	345	0.027	707	5.01	1.41	79.0e6	0.700
3, Fig. 6	0.005	0.995	180	28.3	340	0.024	714	5.00	1.40	79.7e6	0.708
4	0.000	1.000	180	28.0	340	0.023	715	5.00	1.40	79.8e6	0.709

[a] X_{Kr} and X_{N_2} are the Kr and N_2 mole fractions, respectively. P_R is the effective reservoir pressure, and W is the mean molar mass of the mixture. P_w, ρ_w, V_w, M_w, γ_w, Re_w^{unit}, and Pr_w are the static pressure, density, velocity, Mach number, ratio of specific heats, unit Reynolds number, and Prandtl number calculated per the empirical fit in Crist *et al.* [69] at the write location of the underexpanded jet.

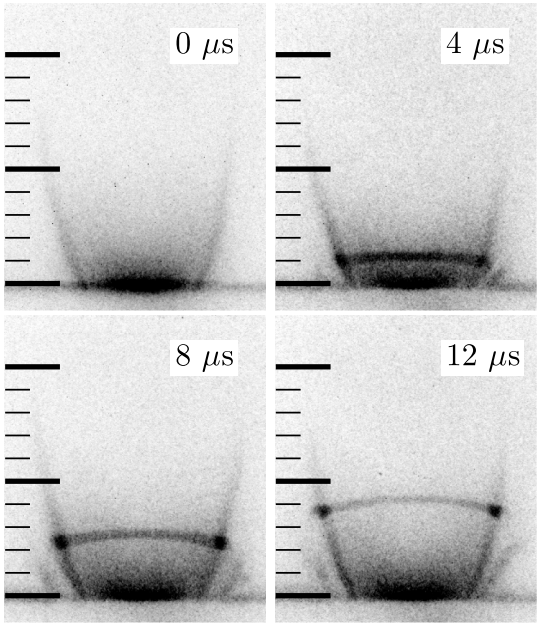

Fig. 4. Case 1. KTV in a 100% krypton underexpanded jet. Inverted intensity scale. Conditions in Table 1. The camera gate is fixed to 20 μs to include the write and read laser pulses. The time stamp of the delay between the write and read pulses is given in μs. Major tick marks are shown at 5 mm intervals.

as Fig. 6. In this series, the camera gate (100 ns) is chosen to bracket only the spontaneous emission from the tagged Kr tracer (after the first image).

7. REDUCTION OF KTV DATA

A time-of-flight style analysis is used to calculate the one-dimensional (1D) velocity of the tagged Kr along the centerline of the underexpanded jet. In the interest of exploring the limits of the technique, the 0.5% Kr/99.5% N_2 case will be analyzed because of its lower SNR ratio relative to the other experiments.

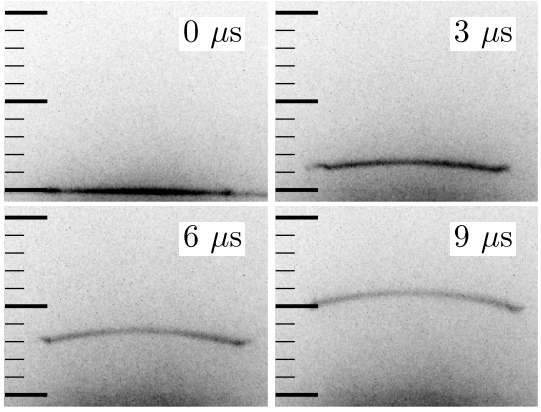

Fig. 5. Case 2. KTV in a 5% Kr/95% N_2 mole fraction underexpanded jet. Inverted intensity scale. Conditions in Table 1. The camera gate is fixed to include only the read laser pulses (after the first image). The time stamp of the delay between the write and read pulse is given in μs. Major tick marks are shown at 5 mm intervals.

The camera response is averaged along a 375 μm (10 pixel) slice on the centerline to track the tagged krypton (left to right in each exposure of Fig. 6). The slice width is less than 1% of the radius of curvature of the tagged Kr (computed by image processing in MATLAB); thus, two-dimensional effects need not be considered. The averaging of this slice along the centerline yields a 1D intensity vector for each exposure; these are denoted with diamond markers in Fig. 7.

To find the tagged Kr center-of-mass location, a Gaussian model of the form $f(x) = a\ \exp(-((x-b)/c)^2)$ is fitted to the intensity vector for each exposure. The centroid (b) and the 95% confidence bounds are determined with MATLAB. The traversed distance, Δx, is then found as the read-centroid location relative to the write-centroid location. The Gaussian fits (solid lines) are presented in addition to the experimental intensity vectors (diamond markers) in Fig. 7. Each centroid is marked with a circle, and the color of each plot corresponds to the color-mark in the lower right of each image in Fig. 6. For example, the write location (black) and a read location (green) were determined from the intensity data in Fig. 7, and these correspond to the upper-left, and lower-right images in Fig. 6 at 0 and 3000 ns, respectively. The time-of-flight, Δt, is the prescribed delay between the write- and read-laser Q-switch pulses.

Velocity is then found as $V = \Delta x/\Delta t$ (Fig. 8). Implicit in this formulation is that the local acceleration is small. The velocities presented in Fig. 8 are plotted with the corresponding colors to Fig. 7 and the color mark in the lower-right corner of each exposure in Fig. 6. The velocity data appearing in Fig. 8 denoted by thin black markers are from the same data set, but are omitted from Figs. 6 and 7 for clarity of the data-reduction presentation.

The uncertainty in the experimental velocimetry results in Fig. 8 is determined in the usual manner [71]. The uncertainty in Δx is estimated as the 95% confidence bound around the Gaussian centroid determined for each vector of averaged

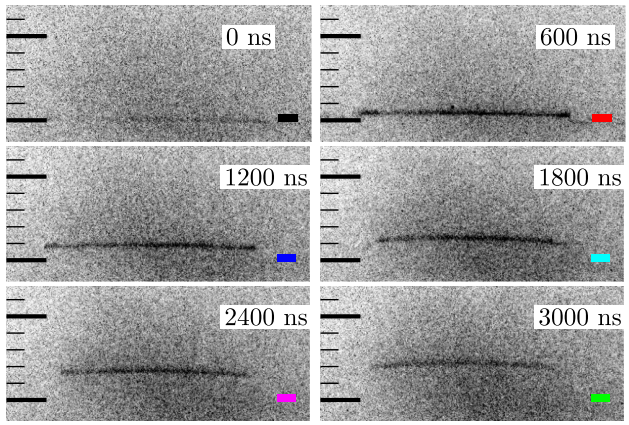

Fig. 6. Case 3. KTV in a 0.5% Kr/99.5% N_2 mole fraction underexpanded jet. Inverted intensity scale. Conditions in Table 1. The camera gate is fixed to include only the read laser pulses (after the first image). The time stamp of the delay between the write and read pulses is given in ns. Major tick marks are shown at 5 mm intervals. The color marks in the lower-right corner of each exposure correspond to the colors of the data presented in Figs. 7 and 8.

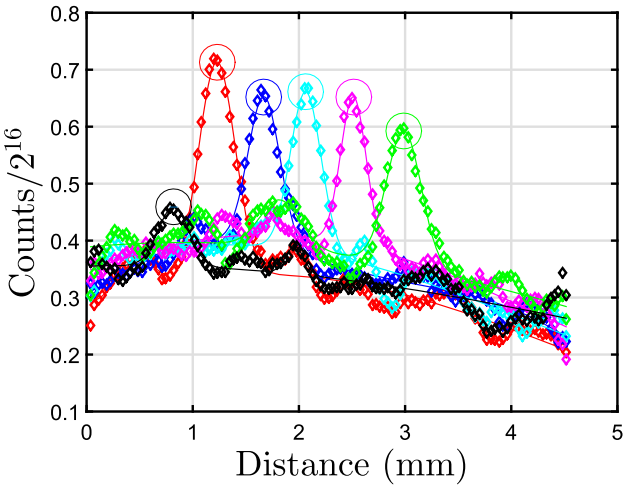

Fig. 7. Processed data from exposures in Fig. 6. The intensity vectors are denoted by diamond markers, and the Gaussian fits to the data are marked by solid lines of the same color. The circles mark the centroid of the intensity data, per the Gaussian fits. Colors marking the processed image data presented here and in Fig. 8 correspond to the color marks in the lower-right corner of each exposure in Fig. 6.

image intensity. The uncertainty in Δt is estimated to be 50 ns, primarily due to fluorescence blurring as considered in Bathel *et al.* [28]. From the manufacturer's specification, we estimate that the jitter is relatively small, approximately 1 ns for each laser. The fluorescence blurring primarily occurs because of the time scale associated with the $5p[3/2]_2 \rightarrow 5s[3/2]_1^o$ and $5p[3/2]_2 \rightarrow 5s[3/2]_2^o$ transitions (25 ns [64–67]). We double this value and report that as the uncertainty in Δt. Additionally, the uncertainty due to the predicted local acceleration of the gas (3%) is included in a root-means-squares sense. As expected, due to the functional form of the velocity relation ($V = \Delta x/\Delta t$), the magnitude of the error bars decrease with increasing distance from the write location. The uncertainty in the velocimetry results is below 5% at nondimensional distances of greater than $x/D_j \approx 2.75$. These values of uncertainty are indicative of a strength of the KTV technique: the lifetime of the metastable Kr state is long enough to yield velocimetry results with reasonably low uncertainty. The empirical fit of Crist *et al.* [69] (black line in Fig. 8) falls within the error bars of the KTV data, bringing confidence to the results.

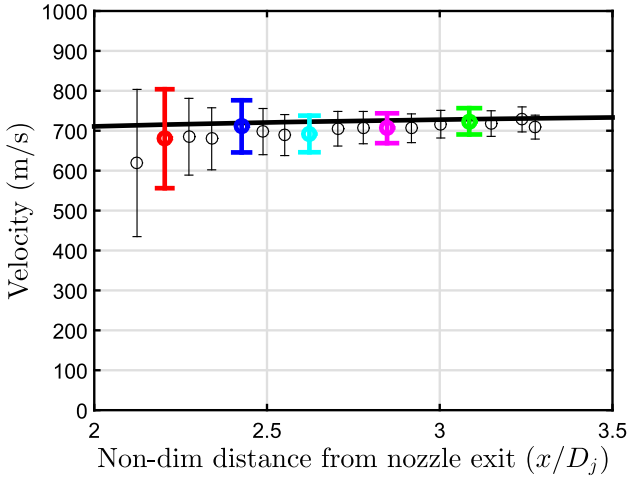

Fig. 8. KTV in a 0.5% Kr/99.5% N_2 mole fraction underexpanded jet. The circular markers are experimental KTV data and the solid line is an empirical fit from Crist *et al.* [69]. Colors marking the processed image data presented here and in Fig. 7 correspond to the color marks in the lower-right corner of each exposure in Fig. 6.

8. CONCLUSIONS AND FUTURE WORK

In this work, KTV is performed in an underexpanded jet. The experimental setup and excitation/emission scheme of krypton for tagging velocimetry are presented. The data reduction scheme is described, and the uncertainty is estimated. A comparison of the experimental KTV data is found to compare favorably to an empirical fit from Crist *et al.* [69].

We demonstrate that the KTV technique can be used in gas mixtures with relatively low krypton mole fraction (0.5% Kr/99.5% N_2). Importantly, the uncertainty in the velocimetry results was found to be less than 5% for times of flight (Δt) shorter than the metastable decay time. Additionally, the uncertainty in the velocimetry results could be reduced with refined treatment of the experimental setup. We conclude that the KTV technique shows promise as a velocimetry tool with tagged krypton as a chemically-inert, dilute, long-lifetime tracer in gas-phase flows.

In the future, we believe that the KTV technique has the potential to broaden the utility of tagging velocimetry with new applications to reacting flows because of the chemically inert nature of the tracer. The utility of the technique will need to be demonstrated in the study of flows of larger characteristic scale than the small underexpanded jet examined in this work. In addition, the lifetime of the metastable Kr tracer will need to be quantified in flows of varying chemical composition and thermodynamic state.

The Air Force SFFP supported Parziale with a stipend for this work. The facilities and equipment were supplied by the Arnold Engineering Development Center (AEDC). We would like to acknowledge the encouragement of John Laffery and Dan Marren of AEDC White Oak. We would also like to acknowledge Joseph Wehrmeyer at Aerospace Testing Alliance (AEDC) for providing some of the laser systems.

USAF Summer Faculty Fellowship Program.

REFERENCES

1. C. Tropea, A. L. Yarin, and J. F. Foss, *Springer Handbook of Experimental Fluid Mechanics* (Springer, 2007).
2. M. M. Koochesfahani and D. G. Nocera, "Molecular tagging velocimetry," in *Springer Handbook of Experimental Fluid Mechanics*, C. Tropea, A. L. Yarin, and J. F. Foss, eds. (Springer, 2007).
3. R. Miles, C. Cohen, J. Connors, P. Howard, S. Huang, E. Markovitz, and G. Russell, "Velocity measurements by vibrational tagging and fluorescent probing of oxygen," Opt. Lett. **12**, 861–863 (1987).
4. R. Miles, J. Connors, E. Markovitz, P. Howard, and G. Roth, "Instantaneous profiles and turbulence statistics of supersonic free shear layers by Raman excitation plus laser-induced electronic fluorescence (RELIEF) velocity tagging of oxygen," Exp. Fluids **8**, 17–24 (1989).

5. R. B. Miles, D. Zhou, B. Zhang, and W. R. Lempert, "Fundamental turbulence measurements by RELIEF flow tagging," AIAA J. **31**, 447–452 (1993).
6. R. B. Miles and W. R. Lempert, "Quantitative flow visualization in unseeded flows," Annu. Rev. Fluid Mech. **29**, 285–326 (1997).
7. R. B. Miles, J. Grinstead, R. H. Kohl, and G. Diskin, "The RELIEF flow tagging technique and its application in engine testing facilities and for helium-air mixing studies," Meas. Sci. Technol. **11**, 1272–1281 (2000).
8. R. W. Pitz, T. M. Brown, S. P. Nandula, P. A. Skaggs, P. A. DeBarber, M. S. Brown, and J. Segall, "Unseeded velocity measurement by ozone tagging velocimetry," Opt. Lett. **21**, 755–757 (1996).
9. L. A. Ribarov, J. A. Wehrmeyer, F. Batliwala, R. W. Pitz, and P. A. DeBarber, "Ozone tagging velocimetry using narrowband excimer lasers," AIAA J. **37**, 708–714 (1999).
10. R. W. Pitz, J. A. Wehrmeyer, L. A. Ribarov, D. A. Oguss, F. Batliwala, P. A. DeBarber, S. Deusch, and P. E. Dimotakis, "Unseeded molecular flow tagging in cold and hot flows using ozone and hydroxyl tagging velocimetry," Meas. Sci. Technol. **11**, 1259–1271 (2000).
11. J. B. Michael, M. R. Edwards, A. Dogariu, and R. B. Miles, "Femtosecond laser electronic excitation tagging for quantitative velocity imaging in air," Appl. Opt. **50**, 5158–5162 (2011).
12. N. Dam, R. J. H. Klein-Douwel, N. M. Sijtsema, and J. J. ter Meulen, "Nitric oxide flow tagging in unseeded air," Opt. Lett. **26**, 36–38 (2001).
13. N. M. Sijtsema, N. J. Dam, R. J. H. Klein-Douwel, and J. J. ter Meulen, "Air photolysis and recombination tracking: a new molecular tagging velocimetry scheme," AIAA J. **40**, 1061–1064 (2002).
14. W. P. N. Van der Laan, R. A. L. Tolboom, N. J. Dam, and J. J. ter Meulen, "Molecular tagging velocimetry in the wake of an object in supersonic flow," Exp. Fluids **34**, 531–534 (2003).
15. S. Krüger and G. Grünefeld, "Stereoscopic flow-tagging velocimetry," Appl. Phys. B **69**, 509–512 (1999).
16. C. Orlemann, C. Schulz, and J. Wolfrum, "NO-flow tagging by photodissociation of NO_2. A new approach for measuring small-scale flow structures," Chem. Phys. Lett. **307**, 15–20 (1999).
17. A. G. Hsu, R. Srinivasan, R. D. W. Bowersox, and S. W. North, "Molecular tagging using vibrationally excited nitric oxide in an underexpanded jet flowfield," AIAA J. **47**, 2597–2604 (2009).
18. A. G. Hsu, R. Srinivasan, R. D. W. Bowersox, and S. W. North, "Two-component molecular tagging velocimetry utilizing NO fluorescence lifetime and NO_2 photodissociation techniques in an underexpanded jet flowfield," Appl. Opt. **48**, 4414–4423 (2009).
19. R. Sánchez-González, R. Srinivasan, R. D. W. Bowersox, and S. W. North, "Simultaneous velocity and temperature measurements in gaseous flow fields using the venom technique," Opt. Lett. **36**, 196–198 (2011).
20. R. Sánchez-González, R. D. W. Bowersox, and S. W. North, "Simultaneous velocity and temperature measurements in gaseous flowfields using the vibrationally excited nitric oxide monitoring technique: a comprehensive study," Appl. Opt. **51**, 1216–1228 (2012).
21. N. Jiang, M. Nishihara, and W. R. Lempert, "Quantitative NO_2 molecular tagging velocimetry at 500 kHz frame rate," Appl. Phys. Lett. **97**, 221103 (2010).
22. N. Jiang, M. Nishihara, and W. R. Lempert, "500 kHz NO_2 molecular tagging velocimetry in a Mach 5 wind tunnel," in *27TH AIAA Aerodynamics Measurement Technology and Ground Testing Conference (AIAA-2010-4348)*, Chicago, Illinois, 2010.
23. B. F. Bathel, C. T. Johansen, P. M. Danehy, J. A. Inman, and S. B. Jones, "Hypersonic boundary layer transition measurements using $NO_2 \rightarrow NO$ photo-dissociation tagging velocimetry," in *Proceedings of 41st AIAA Fluid Dynamics Conference and Exhibit (AIAA-2011-3246)*, Honolulu, Hawaii, 2011.
24. A. M. ElBaz and R. W. Pitz, "N_2O molecular tagging velocimetry," Appl. Phys. B **106**, 961–969 (2012).
25. J. A. Inman, P. M. Danehy, B. F. Bathel, and R. J. Nowak, "Laser-induced fluorescence velocity measurements in supersonic underexpanded impinging jets," in *Proceedings of 48th AIAA Aerospace Sciences Meeting and Exhibit AIAA-2010-1438*, Orlando, Florida, 2010.
26. B. F. Bathel, P. M. Danehy, J. A. Inman, S. B. Jones, C. B. Ivey, and C. P. Goyne, "Multiple velocity profile measurements in hypersonic flows using sequentially-imaged fluorescence tagging," in *Proceedings of 48th AIAA Aerospace Sciences Meeting Including the New Horizons Forum and Aerospace Exposition (AIAA-2010-1404)*, Orlando, Florida, 2010.
27. B. F. Bathel, P. M. Danehy, J. A. Inman, A. N. Watkins, S. B. Jones, W. E. Lipford, and K. Z. Goodman, "Hypersonic laminar boundary layer velocimetry with discrete roughness on a flat plate," in *Proceedings of 40th AIAA Fluid Dynamics Conference and Exhibit (AIAA-2010-4998)*, Chicago, Illinois, 2010.
28. B. F. Bathel, P. M. Danehy, J. A. Inman, S. B. Jones, C. B. Ivey, and C. P. Goyne, "Velocity profile measurements in hypersonic flows using sequentially imaged fluorescence-based molecular tagging," AIAA J. **49**, 1883–1896 (2011).
29. R. Sánchez-González, R. D. W. Bowersox, and S. W. North, "Vibrationally excited NO tagging by $NO(A^2\Sigma^+)$ fluorescence and quenching for simultaneous velocimetry and thermometry in gaseous flows," Opt. Lett. **39**, 2771–2774 (2014).
30. P. M. Danehy, P. Mere, M. J. Gaston, S. O'Byrne, P. C. Palma, and A. F. P. Houwing, "Fluorescence velocimetry of the hypersonic, separated flow over a cone," AIAA J. **39**, 1320–1328 (2001).
31. S. O'Byrne, P. M. Danehy, and A. F. P. Houwing, "Nonintrusive temperature and velocity measurements in a hypersonic nozzle flow," in *Proceedings of 22nd AIAA Aerodynamic Measurement Technology and Ground Testing Conference (AIAA-2002-2917)*, St. Louis, Missouri, 2002.
32. P. M. Danehy, S. O'Byrne, A. F. P. Houwing, J. S. Fox, and D. R. Smith, "Flow-tagging velocimetry for hypersonic flows using fluorescence of nitric oxide," AIAA J. **41**, 263–271 (2003).
33. J. C. McDaniel, B. Hiller, and R. K. Hanson, "Simultaneous multiple-point velocity measurements using laser-induced iodine fluorescence," Opt. Lett. **8**, 51–53 (1983).
34. R. J. Balla, "Iodine tagging velocimetry in a Mach 10 wake," AIAA J. **51**, 1783–1786 (2013).
35. W. R. Lempert, N. Jiang, S. Sethuram, and M. Samimy, "Molecular tagging velocimetry measurements in supersonic microjets," AIAA J. **40**, 1065–1070 (2002).
36. W. R. Lempert, M. Boehm, N. Jiang, S. Gimelshein, and D. Levin, "Comparison of molecular tagging velocimetry data and direct simulation Monte Carlo simulations in supersonic micro jet flows," Exp. Fluids **34**, 403–411 (2003).
37. T. Handa, K. Mii, T. Sakurai, K. Imamura, S. Mizuta, and Y. Ando, "Study on supersonic rectangular microjets using molecular tagging velocimetry," Exp. Fluids **55**, 1–11 (2014).
38. L. R. Boedeker, "Velocity measurement by H_2O photolysis and laser-induced fluorescence of OH," Opt. Lett. **14**, 473–475 (1989).
39. J. A. Wehrmeyer, L. A. Ribarov, D. A. Oguss, and R. W. Pitz, "Flame flow tagging velocimetry with 193-nm H_2O photodissociation," Appl. Opt. **38**, 6912–6917 (1999).
40. R. W. Pitz, M. D. Lahr, Z. W. Douglas, J. A. Wehrmeyer, S. Hu, C. D. Carter, K.-Y. Hsu, C. Lum, and M. M. Koochesfahani, "Hydroxyl tagging velocimetry in a supersonic flow over a cavity," Appl. Opt. **44**, 6692–6700 (2005).
41. B. Hiller, R. A. Booman, C. Hassa, and R. K. Hanson, "Velocity visualization in gas flows using laser-induced phosphorescence of biacetyl," Rev. Sci. Instrum. **55**, 1964–1967 (1984).
42. C. P. Gendrich and M. M. Koochesfahani, "A spatial correlation technique for estimating velocity fields using molecular tagging velocimetry (MTV)," Exp. Fluids **22**, 67–77 (1996).
43. C. P. Gendrich, M. M. Koochesfahani, and D. G. Nocera, "Molecular tagging velocimetry and other novel applications of a new phosphorescent supramolecule," Exp. Fluids **23**, 361–372 (1997).
44. B. Stier and M. M. Koochesfahani, "Molecular tagging velocimetry (MTV) measurements in gas phase flows," Exp. Fluids **26**, 297–304 (1999).
45. J. L. Mills, C. I. Sukenik, and R. J. Balla, "Hypersonic wake diagnostics using laser induced fluorescence techniques," in *Proceedings of 42nd AIAA Plasmadynamics and Lasers Conference (AIAA 2011-3459)*, Honolulu, Hawaii, 2011.
46. R. J. Balla and J. L. Everhart, "Rayleigh scattering density measurements, cluster theory, and nucleation calculations at Mach 10," AIAA J. **50**, 698–707 (2012).

47. V. Narayanaswamy, R. Burns, and N. T. Clemens, "Kr-PLIF for scalar imaging in supersonic flows," Opt. Lett. **36**, 4185–4187 (2011).
48. A. G. Hsu, V. Narayanaswamy, N. T. Clemens, and J. H. Frank, "Mixture fraction imaging in turbulent non-premixed flames with two-photon LIF of krypton," Proc. Combust. Inst. **33**, 759–766 (2011).
49. E. B. Saloman, "Energy levels and observed spectral lines of krypton, Kr I through Kr XXXVI," J. Phys. Chem. Ref. Data **36**, 215–386 (2007).
50. O. R. H. Buxton, R. A. Burns, and N. T. Clemens, "Simultaneous krypton PLIF, LII and PIV measurements in a sooting jet flame," in *Proceedings of 51st AIAA Aerospace Sciences Meeting including the New Horizons Forum and Aerospace Exposition (AIAA-2013-0479)*, Grapevine, Texas, 2013.
51. H. Katori and F. Shimizu, "Lifetime measurement of the $1s_5$ metastable state of argon and krypton with a magneto-optical trap," Phys. Rev. Lett. **70**, 3545–3548 (1993).
52. J. Lefers, N. Miller, D. Rupke, D. Tong, and M. Walhout, "Direct measurement of the metastable 3P2 decay rate in krypton," Phys. Rev. A **66**, 012507 (2002).
53. C. J. Tracy and H. Oskam, "Properties of metastable krypton atoms in afterglows produced in krypton and krypton–nitrogen mixtures," J. Chem. Phys. **65**, 1666–1671 (1976).
54. J. E. Velazco, J. H. Kolts, and D. W. Setser, "Rate constants and quenching mechanisms for the metastable states of argon, krypton, and xenon," J. Chem. Phys. **69**, 4357–4373 (1978).
55. R. Sobczynski and D. W. Setser, "Improvements in the generation and detection of $Kr(^3P_0)$ and $Kr(^3P_2)$ atoms in a flow reactor: decay constants in He buffer and total quenching rate constants for Xe, N_2, CO, H_2, CF_4, and CH_4," J. Chem. Phys. **95**, 3310–3324 (1991).
56. D. A. Zayarnyi, A. Yu L'dov, and I. V. Kholin, "Deactivation of krypton atoms in the metastable $5s(^3P_2)$ state in collisions with krypton and argon atoms," Quantum Electron. **39**, 821 (2009).
57. D. Marren and J. Lafferty, "The AEDC hypervelocity wind tunnel 9," in *Advanced Hypersonic Test Facilities* (American Institute of Aeronautics and Astronautics, 2002), pp. 467–478.
58. D. G. Goodwin, "An open-source, extensible software suite for cvd process simulation," in *Proceedings of CVD XVI and EuroCVD Fourteen*, M. Allendorf, F. Maury, and F. Teyssandier, eds. (2003), pp. 155–162.
59. S. Chapman and T. G. Cowling, *The Mathematical Theory of Non-uniform Gases* (Cambridge University, 1939).
60. B. J. McBride, M. J. Zehe, and S. Gordon, "NASA Glenn coefficients for calculating thermodynamic properties of individual species," NASA TP-2002-211556 (2002).
61. J. O. Hirschfelder, C. F. Curtiss, and R. B. Bird, *Molecular Theory of Gases and Liquids* (Wiley, 1954).
62. D. McQuarrie, *Statistical Mechanics* (University Science Books, 2000).
63. J. C. Miller, "Two-photon resonant multiphoton ionization and stimulated emission in krypton and xenon," Phys. Rev. A **40**, 6969–6976 (1989).
64. V. Fonseca and J. Campos, "Absolute transition probabilities of some Kr I lines," Physica B + C **97**, 312–314 (1979).
65. R. S. F. Chang, H. Horiguchi, and D. W. Setser, "Radiative lifetimes and two–body collisional deactivation rate constants in argon for Kr ($4p^55p$) and Kr($4p^55p'$) states," J. Chem. Phys. **73**, 778–790 (1980).
66. C. A. Whitehead, H. Pournasr, M. R. Bruce, H. Cai, J. Kohel, W. B. Layne, and J. W. Keto, "Deactivation of two-photon excited Xe ($5p^56p,6p',7p$) and Kr($4p^55p$) in xenon and krypton," J. Chem. Phys. **102**, 1965–1980 (1995).
67. K. Dzierżega, U. Volz, G. Nave, and U. Griesmann, "Accurate transition rates for the 5p-5s transitions in Kr I," Phys. Rev. A **62**, 022505 (2000).
68. C. E. Smith, "The starting process in a hypersonic nozzle," J. Fluid Mech. **24**, 625–640 (1966).
69. S. Crist, D. R. Glass, and P. M. Sherman, "Study of the highly underexpanded sonic jet," AIAA J. **4**, 68–71 (1966).
70. H. W. Liepmann and A. Roshko, *Elements of Gasdynamics* (Wiley, 1957).
71. R. J. Moffat, "Describing the uncertainties in experimental results," Exp. Therm. Fluid. Sci. **1**, 3–17 (1988).